Valence Fluctuations and Metallic Behavior in $K_6Cu_{12}U_2S_{15}$, a New Quaternary Sulfide with a Unique Three-Dimensional Cubic Framework

Anthony C. Sutorik,[a] Rhonda Patschke,[a] Jon Schindler,[b] Carl R. Kannewurf,[b] and Mercouri G. Kanatzidis*[a]

Abstract: Mixed S^{2-}/S^{1-} oxidation states have been discovered in the new quaternary compound $K_6Cu_{12}U_2S_{15}$. Synthesized from the reaction of Cu and U in a molten alkali metal/polysulfide flux, the compound crystallizes in the cubic space group $Ia\bar{3}d$ (no. 230) with a = 18.642(7) Å. Its complex structure is built from $[US_6]$ octahedra connected into one-dimensional columns with $[CuS_3]$ trigonal planar units, which also serve as inter-column connection points for the extended three-dimensional structure. Magnetic susceptibility measurements reveal Curie–Weiss paramagnetic behavior at temperatures above 100 K with a μ_{eff} of 2.96 μ_B per formula. This corresponds to 2.1 μ_B per U atom, and it is insufficient to distinguish between U^{4+} and U^{5+} paramagnetic ions. The conductivity of hot-pressed polycrystalline pellets is $\sim 1500\ S\,cm^{-1}$ at room temperature, and increasing conductivity with decreasing temperature is observed, indicating metallic behavior for the material. Small and positive values for the material's thermopower ($3-4\ \mu V\,K^{-1}$ from 100–300 K) also confirm p-type metallic behavior.

Keywords: actinides · conductivity · flux synthesis · metallic sulfides · thermopower · valence fluctuations

Introduction

Among the many known solid-state copper chalcogenides are several unusual phases that feature monochalcogenides with a 1− charge without the formation of chalcogen–chalcogen bonds. These occur in both binary (i.e., CuQ, Q = S, Se, Te)[1] and ternary (i.e., ACu_4Q_3; A = K, Rb, Cs, Tl; Q = S, Se;[2] $NaCu_4S_4$;[3] and $Na_3Cu_4S_4$[4]) systems.[5] When many of these compounds were first discovered, the assumption was that the mixed valence occurred through Cu^{2+}/Cu^{1+} states.[6] However, crystallographic studies invariably showed all Cu atoms to be equivalent with no difference in bond lengths, which would have been expected for two different oxidation states. Subsequent physical studies on these materials (i.e., electrical conductivity measurements[2, 4a] and X-ray photoelectron spectroscopy[1a]) led to the realization that the mixed valency was actually on the Q atoms. This model predicts p-type metallic conductivity due to the Q^{1-} states being delocalized as holes through the valence band. The conductivity of several of these phases is, in fact, significant. For example, single crystals of $Na_3Cu_4S_4$, which feature a structure of one-dimensional $[Cu_4S_4]^{3-}$ chains, have a room temperature conductivity of $15000\ S\,cm^{-1}$ in the direction parallel to the chains.[4a]

In our studies of Cu and f-block metal reactivity in molten polychalcogenide salts, we have observed that mixed S^{2-}/S^{1-} oxidation states can also occur in Cu-containing quaternary phases. For example, $K_2Cu_2CeS_4$ can be described as $(K^{1+})_2(Cu^{1+})_2(Ce^{3+})(S^{2-})_3(S^{1-})$, a formalism confirmed by magnetic susceptibility studies.[7] Similarly, $CsCuCeS_3$ can be expressed as $(Cs^{1+})(Cu^{1+})(Ce^{3+})(S^{2-})_2(S^{1-})$, although in this case magnetic measurements indicated valence fluctuations more complicated than this simple model.[8] Since the (S^{1-}) states in both these compounds are delocalized through the valence band (of primarily sulfur 3p character), metallic behavior would be expected. Charge-transport studies on these compounds confirmed the hole mobility, but indicated complicated, non-metallic conduction mechanisms. This arises in part from the fact that both $K_2Cu_2CeS_4$ and $CsCuCeS_3$ have layered structures in which sheets of covalently bound Cu, Ce, and S atoms are separated by intervening layers of alkali cations. Hence, hole mobility is restricted in the directions perpendicular to the layers, and the width of the valence bands is narrowed relative to structures with three-dimensional covalent bonding. Reduced dimensionality itself, however, is insufficient to account for the charge-transport behavior of these quaternaries because several ternary compounds with mixed S^{2-}/S^{1-} and reduced dimensionality are

[a] Prof. M. G. Kanatzidis, Dr. A. C. Sutorik, R. Patschke
Department of Chemistry, Michigan State University
East Lansing, MI, 48824 (USA)
Fax: (+1) 517-353-1793
E-mail: kanatzid@cem.msu.edu

[b] J. Schindler, Prof. C. R. Kannewurf
Department of Electrical Engineering and Computer Science
Northwestern University, Evanston, Illinois, 60208 (USA)

  0947-6539/00/0609-1601 $ 17.50+.50/0

still metallic.[2, 4a] Another factor serving to narrow the valence bands is the presence of Ce. The bonding of Ce (and lanthanides in general) tends to be very ionic in character; the 4f orbitals are contracted below the shell of core electrons, and the 5d, 6s, and 6p orbitals are too high in energy to effectively interact with the valence band, composed mainly of sulfur 3p orbitals. This limited orbital overlap serves to narrow the valence bands even further, making carrier-limiting phenomena such as small polaron formation more likely.[9] If this explanation is valid, then mixed S^{2-}/S^{1-} in quaternary compounds with non-lanthanide metals, which would have stronger covalent interactions with the bulk structure, should result in phases with greater carrier mobility and metallic behavior, especially if the materials possessed three-dimensional structures.

The new quaternary compound $K_6Cu_{12}U_2S_{15}$ represents just such a material. Its framework is composed of $[US_6]$ octahedra linked into an unprecedented three-dimensional covalent network with intervening $[CuS_3]$ trigonal planar units and K cations residing in tunnels that run through the structure. The strongly covalent 5f orbitals of U combine with the three-dimensional structure to provide exceptional mobility to the delocalized S^{1-} charge carriers. As a result $K_6Cu_{12}U_2S_{15}$ is clearly metallic; the conductivity of pressed polycrystalline pellets is $\sim 1500\ S\,cm^{-1}$ at room temperature, 10^3 and 10^6 times greater than those of $CsCuCeS_3$ and $K_2Cu_2CeS_4$, respectively.

Experimental Section

Reagents: The following reagents were used as obtained: uranium metal (60 mesh, Cerac, Milwaukee, WI), copper metal (Fisher Scientific, Fairlawn, NJ), sulfur powder (sublimed, JT Baker, Phillipsburg, NJ), potassium metal (analytical reagent, Mallinckrodt, Paris, KY), and dimethylformamide (DMF, analytical reagent grade, EM Science, Gibbstown, NJ).

Potassium sulfide (K_2S): The following procedure was modified from that given in the literature.[10] A sample of K (7.092 g, 181 mmol) was cut into small pieces in a N_2-filled glovebox and combined with S (2.908 g, 91 mmol) in a 250 mL round-bottomed flask. The flask was cooled to $-78\,^{\circ}C$ in a dry ice/acetone bath. NH_3 (ca. 100 mL) was condensed onto the reagents under a N_2 atmosphere, to give a dark blue solution. The solution was stirred with a magnetic stir bar, while the liquid NH_3 was allowed to slowly evaporate (approximately 12 h) under a flow of N_2. A second portion of NH_3 was added, and the evaporation process was repeated to ensure complete reaction of the reagents. The resulting yellow product was evacuated on a Schlenk line overnight and placed in a N_2-filled glovebox, where it was ground to a fine powder and stored.

$K_6Cu_{12}U_2S_{15}$: A mixture of K_2S (0.103 g, 0.934 mmol), Cu (0.048 g, 0.75 mmol), U (0.030g, 0.126 mmol), and S (0.120 g, 3.74 mmol) was weighed into a vial in a N_2-filled glovebox. The reactants were mixed thoroughly and loaded into a Pyrex tube, which was evacuated to $>3\times10^{-3}$ mbar and flame-sealed. In a computer-controlled furnace, the mixture was heated to 500 °C over 12 h, held at that temperature for 4 days, and cooled to 100 °C at $4\,^{\circ}C\,h^{-1}$ followed by quenching to 50 °C. The product was isolated by dissolving the residual K_2S_x flux with successive portions of degassed DMF; the dissolution was performed under flowing N_2 to prevent oxidation of polysulfide to sulfur. Polysulfides dissolve in DMF to give a dark blue-green solution; when this color was achieved, the solution was decanted from the solid residue, and a fresh portion of solvent was added. The K_2S_x isolation was considered complete when the DMF solution remained clear. After the final decanting, the black microcrystalline sample of $K_6Cu_{12}U_2S_{15}$ was dried under vacuum, and its identity and purity were confirmed by comparing its X-ray powder diffraction pattern with one calculated by using data from the single-crystal study. Typical yields were 23 %, based on Cu. $K_6Cu_{12}U_2S_{15}$ is insoluble in water, methanol, and DMF and is stable in air for extended periods. Despite the high product purity, this procedure yields only a microcrystalline powder. Crystals of the appropriate size for single-crystal X-ray diffraction were found as a minor phase during attempted studies of uranyl ($[UO_2]^{2+}$) reactivity in excess K_2S_x [K_2S (0.083 g, 0.075 mmol), Cu (0.008 g, 0.126 mmol), U (0.030 g, 0.126 mmol), SeO_2(0.014 g, 0.126 mmol), and S (0.048 g, 1.50 mmol) that was heated at 400 °C for 4 days, cooled to 200 °C at $4\,^{\circ}C\,h^{-1}$, and quenched to 50 °C].[11]

Physical measurements

Powder X-ray diffraction: Powder diffractograms were obtained by using a calibrated Rigaku Rotoflex rotating-anode powder diffractometer, employing Ni-filtered Cu radiation, controlled by an IBM computer, and operated at 45 kV/100 mA. Samples were ground to a fine powder and mounted by spreading the sample onto a piece of double-sided tape affixed to a glass slide. Powder patterns were calculated by using the CERIUS molecular-modeling program by Molecular Simulations (St. John's Innovation Centre, Cambridge, England).

Magnetic susceptibility: The magnetic response of the compound was measured over the range of 2 – 300 K by using an MPMS Quantum Design SQUID magnetometer. Samples were ground to a fine powder to minimize anisotropic effects, and corrections for the diamagnetism of the PVC sample containers and the diamagnetism of the atoms were applied. Magnetic susceptibility as a function of field strength (at a constant temperature of 300 K) was first investigated to determine if the samples experienced saturation of their magnetic signal. For all samples the magnetization increased linearly with increasing field over the range investigated (0 – 10000 G). Subsequent temperature-dependent studies were performed at 5000 G.

Charge-transport measurements: Direct current electrical conductivity and thermoelectric power studies were performed on pellets that were pressed in air at both room temperature and at 270 °C. Conductivity measurements were performed in the usual four-probe geometry with 60 and 25 μm diameter gold wires used for the current and voltage electrodes, respectively. Measurements of the sample cross-sectional area and voltage probe separation were made with a calibrated binocular microscope. Conductivity data were obtained with the computer-automated system described elsewhere.[12] Thermoelectric power measurements were made by using a slow alternating current technique[13] that requires the production of a slowly varying periodic temperature gradient across the samples and measurement of the resulting sample voltage. Samples were suspended between quartz block heaters by 60 μm gold wires thermally grounded to the block with GE 7031 varnish. The gold wires were used to support and conduct heat to the sample, as well as to measure the voltage across the sample that resulted from the applied temperature gradient. The magnitude of the applied temperature gradient was generally 1.0 K. Smaller temperature gradients gave essentially the same result, but with lower sensitivity. In both measurements, the gold electrodes were mounted on the sample with conductive gold paste. Mounted samples were placed under vacuum (10 – 3 Torr) and heated to 320 K for 2 – 4 h to cure the gold contacts. Variable-temperature data (conductivity or thermoelectric power) were acquired during sample warming. The average temperature drift rate during an experiment was kept below $0.3\ K\,min^{-1}$. Multiple variable-temperature runs were carried out for each sample to ensure reproducibility and stability. At a given temperature, reproducibility was within ± 5 %.

Single-crystal diffraction: Intensity data were collected using a Rigaku AFC6S four-circle automated diffractometer equipped with a graphite crystal monochromator. An ω-2θ scan mode was used. Crystal stability was monitored with three standard reflections, whose intensities were checked every 150 reflections. No crystal decay was detected. An empirical absorption correction, based on ψ scans, was applied to all data. The structure was solved by direct methods and refined using the SHELXTL-5.0 software package.[14] The highest peak in the final Fourier difference electron-density map was less than $2.0\ e\,Å^{-3}$. Crystallographic and fractional atomic coordinate data are given in Tables 1 and 2. Further details on the crystal structure investigation may be obtained from the Fachinformationszentrum Karlsruhe, D-76344 Eggenstein-Leopoldshafen, Germany (fax: (+49) 7247-808-666; e-mail: crysdata@fiz-karlsruhe.de), on quoting the depository number CSD-411001.

0947-6539/00/0609-1602 $ 17.50+.50/0 *Chem. Eur. J.* **2000**, *6*, No. 9

Table 1. Crystallographic data and structural analysis for $K_6Cu_{12}U_2S_{15}$.

formula weight	1954.04
crystal habit, color	polyhedra, black
crystal size [mm³]	0.20 × 0.20 × 0.24
crystal system	cubic
space group	$Ia\bar{3}d$
a [Å]	18.642(7)
V [Å³]	6479(4)
Z	8
ρ_{calcd} [g cm^{-3}]	4.007
μ [cm^{-1}]	19.392
λ ($Mo_{K\alpha}$) [Å]	0.71073
$2\theta_{max}$ [°]	50.0
T [°C]	23
no. reflections measured	605
no. unique reflections	483
parameters	30
$R1/wR2$[a]	4.35/12.84
GOF on F^2	0.970

[a] $R1 = \Sigma(|F_o| - |F_c|)/\Sigma|F_o|$ [for $I > 2\sigma(I)$]; $wR2 = \{\Sigma[w(F_o^2 - F_c^2)^2]/\Sigma[w(F_o^2)^2]\}^{1/2}$ (for all data).

Table 2. Atomic coordinates ($\times 10^4$), equivalent isotropic displacement parameters (Å$^2 \times 10^3$) for $K_6Cu_{12}U_2S_{15}$.

	multiplicity, Wycoff letter	x	y	z	U(eq)[a]
U(1)	16a	0	0	0	12(1)
Cu(1)	96h	1427(2)	760(2)	77(2)	23(1)
K(1)	48g	−329	1250	2829(3)	32(2)
S(1)	96h	−1277(3)	384(3)	−434(3)	21(1)
S(2)	24c	2500	1250	0	17(2)

[a] U(eq) is defined as one third of the trace of the orthogonalized U_{ij} tensor.

Results and Discussion

$K_6Cu_{12}U_2S_{15}$ structure: The complex, yet elegant, structure of $K_6Cu_{12}U_2S_{15}$ is built from a simple repeating unit composed of a [US_6] octahedron connected to six [CuS_3] trigonal planar units (Figure 1). Each [CuS_3] trigonal plane shares an edge with the [US_6] octahedra; three [CuS_3] units are located on one face of the octahedra, and the remaining three are located on the opposite face. Only the S(1) atoms are bound to the U. The S(2) atoms form corner-sharing bridges to the trigonal planes of the neighboring repeat unit, and this pattern results in 1-dimensional columns as shown in Figure 1. Furthermore, each S(2) atom simultaneously bridges two more trigonal planes in a neighboring column and thus acts as a point of extended connectivity in the structure. The coordination about the S(2) atoms is a distorted tetrahedron with an angle between opposite edges, and hence between neighboring columns, of 110.51°. Figure 2 highlights two neighboring columns connected by an S(2) atom. Each set of three S(2) atoms on a central column makes three bridges to three other columns, and the inter-column connectivity is further complicated because the direction of the tilt between the columns is reversed with each set of S(2) connections.

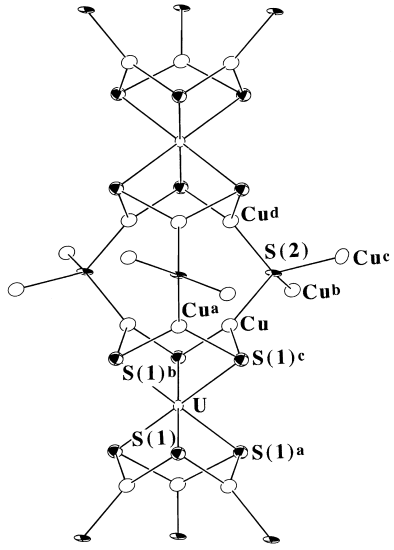

Figure 1. A fragment of the one-dimensional columns of $K_6Cu_{12}U_2S_{15}$ formed by corner-sharing connections at the S(2) atom between neighboring building blocks. The basic building block is a [US_6] octahedron edge-sharing with six [CuS_3] trigonal planes.

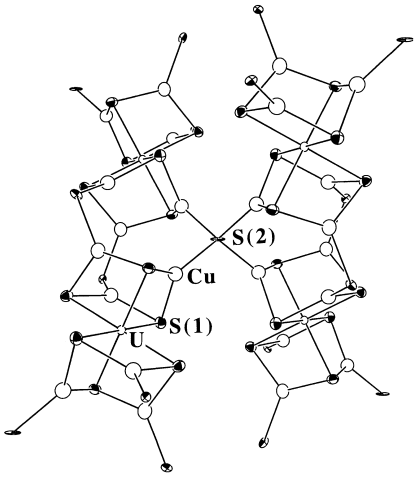

Figure 2. A fragment of the structure highlighting the coordination about an S(2) atom, which serves as the connection point between two columns.

This complex interweaving of columns continues through three dimensions, and one view of the result is given in Figure 3a. From the direction parallel to the *a* axis, we see small channels running through the structure that house the K^+ ions. Since the cell is cubic, these channels run in all three dimensions. Each unit cell contains fragments of seven columns: a central column running from the origin through [1 1 1] and six columns connecting from it at the S(2) atoms (Figure 3b). Each of the columns is symmetry equivalent and so possesses the same connectivity. Figure 4 shows both the crystal structure and a simplified schematic of the unit cell as seen in the [1 $\bar{1}$ 0] direction. These views highlight the central column running along the [1 1 1] direction with a nest of neighboring columns wrapped around its midsection. Finally, Figures 5a and 5b show the view down one of the corners of the cell, in this case the [1 $\bar{1}$ 1] direction. This provides an end on view of the two columns that are approximately parallel to the [2 $\bar{1}$ 1] direction. From all of these views, it can be seen that the K^+ ions are always outside the anionic columns; the pocket formed inside the column between the corner-sharing [CuS_3] units remains void.

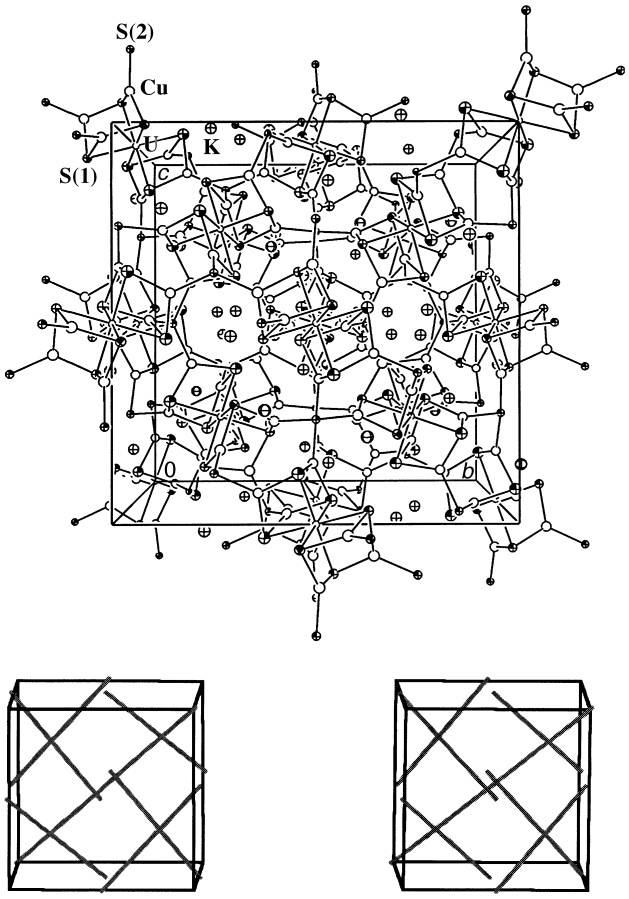

Figure 3. a) The unit cell of $K_6Cu_{12}U_2S_{15}$ as seen parallel to the *a* axis and b) a simplified stereoview from the same direction highlighting the central axes of the structure's interwoven columns.

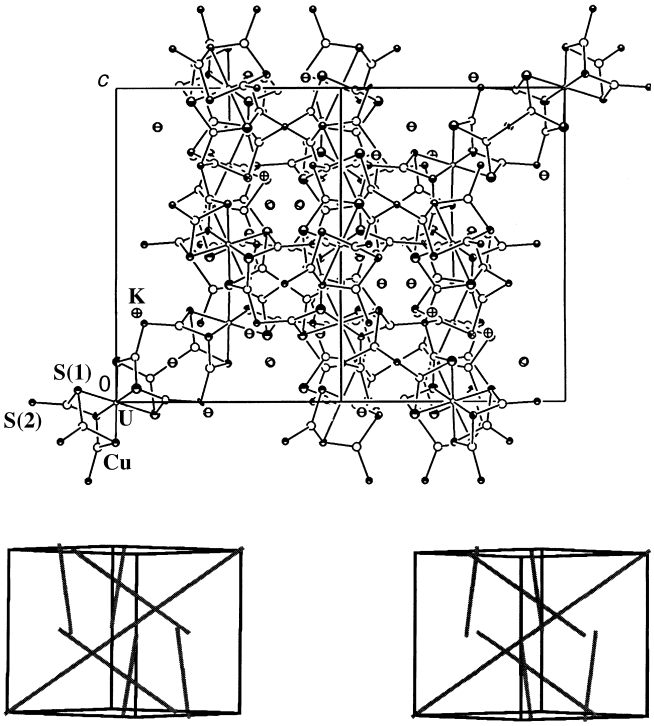

Figure 4. a) The unit cell of $K_6Cu_{12}U_2S_{15}$ as seen parallel to $[1\,\bar{1}\,0]$ and b) a simplified stereoview from the same direction highlighting the central axes of the structure's interwoven columns.

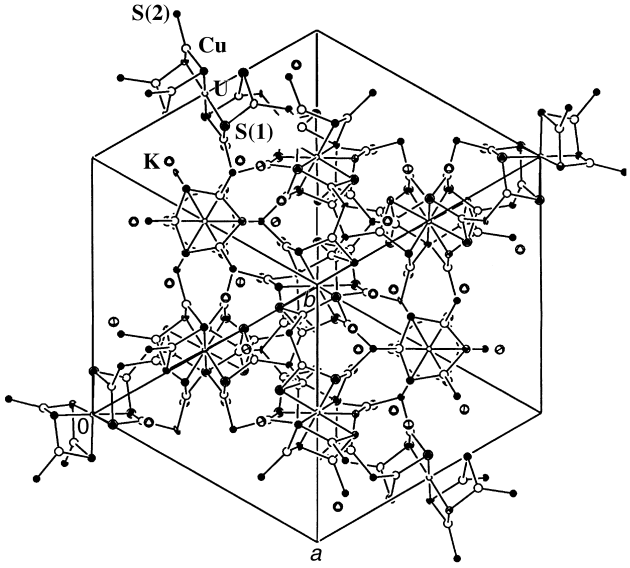

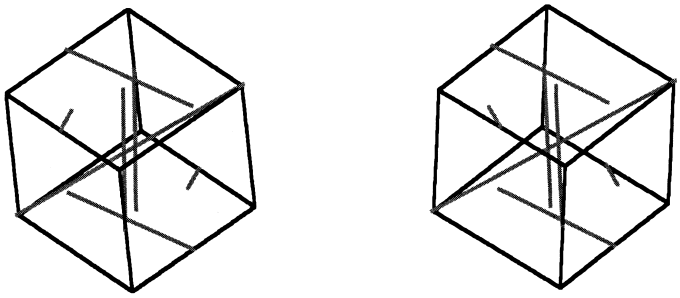

Figure 5. a) The unit cell of $K_6Cu_{12}U_2S_{15}$ as seen parallel to $[1\,\bar{1}\,1]$ and b) a simplified stereoview from the same direction highlighting the central axes of the structure's interwoven columns.

Selected bond lengths for $K_6Cu_{12}U_2S_{15}$ are given in Table 3. All U–S distances are equivalent at 2.615(6) Å, which is slightly shorter than those common to a six-coordinate U^{4+} atom. For example, in $BaUS_3$, which has a distorted perovskite structure, the U–S bond lengths range from 2.680(5) – 2.709(5) Å.[15] Bond angles about the $[US_6]$ octahedra in $K_6Cu_{12}U_2S_{15}$ are nearly ideal, with S-U-S angles defined by S atoms in the face perpendicular to the column direction being slightly larger (S(1)-U-S(1)^a: 93.0(2)°) than the "*trans*-facial" angles (S(1)-U-S(1)^b: 87.0(2)°). The Cu–S bond lengths are 2.204(3) and 2.256(7) Å. For a trigonal planar Cu atom, these bonds are not unusual. In CuS, such bond lengths are slightly shorter at 2.192 Å,[16] and trigonal planar Cu atoms in $CsCuTeS_3$ have bonds to S at 2.245 Å.[17]

Table 3. Selected bond lengths [Å] and angles [°] for $K_6Cu_{12}U_2S_{15}$ with standard deviations in parentheses.

U–Cu	3.017(3)	Cu–S(1)	2.256(7)
U–S(1)	2.615(6)	Cu–S(2)	2.204(3)
U–U	8.072(5)	Cu–Cu	3.082(5)
S(1)-U-S(1)	93.0(2)	U-S(1)-Cu	76.2(2)
S(1)-U-S(1)	180.0	Cu-S(1)-Cu	86.2(3)
S(1)-U-S(1)	87.0(2)	Cu-S(2)-Cu	106.8(2)
S(1)-Cu-S(1)	114.6(3)	Cu-S(2)-Cu	131.1(1)
S(1)-Cu-S(2)	122.9(2)	Cu-S(2)-Cu	93.2(2)
S(1)-Cu-S(2)	121.6(2)	Cu-S(2)-Cu	106.8(2)

0947-6539/00/0609-1604 $ 17.50+.50/0 *Chem. Eur. J.* **2000**, *6*, No. 9

The most unusual distance in $K_6Cu_{12}U_2S_{15}$ is that between U atoms and nearest neighbor Cu atoms at 3.017(3) Å. A similar short distance was observed in $Cu_2U_6S_{13}$ at 3.186 Å,[18a] in which the structure features eight-coordinate uranium in either bicapped trigonal prisms or triangulated dodecahedra and Cu^{1+} ions in trigonal planar sites. In the intermetallic compound UCu_5, the U atoms are 16-coordinate, with twelve U–Cu bond lenghts of 2.92 Å and four of 3.05 Å.[18b] Hence, the short distances in $K_6Cu_{12}U_2S_{15}$ imply some degree of direct U–Cu bonding. If the coordination to Cu is also considered, the U atoms of $K_6Cu_{12}U_2S_{15}$ become 12-coordinate, and the six Cu atoms form a trigonal antiprism (i.e., an octahedron elongated along the columnar axis) about the central U atom; this partially encloses the smaller $[US_6]$ octahedron.

The formal charges on $K_6Cu_{12}U_2S_{15}$ cannot be balanced by using entirely S^{2-} without invoking some combination of Cu^{2+}, U^{5+}, or U^{6+} to achieve charge neutrality. Cu^{2+} is strongly oxidizing relative to S^{2-}, and U^{5+} in a chalcogenide environment is rare, although not without precedent.[19] Like Cu^{2+}, U^{6+} is far too oxidizing to exist in an exclusively chalcogenide environment, but $[UO_2]^{2+}$-containing sulfides have been stabilized.[20] Depending on the occurrence of U^{5+}, three stoichiometric mixed-valent formalisms can be written: $(K^+)_6(Cu^+)_{12}(U^{4+})_2(S^{2-})_{11}(S^{1-})_4$, $(K^+)_6(Cu^+)_{12}(U^{4+})(U^{5+})(S^{2-})_{12}(S^{1-})_3$, and $(K^+)_6(Cu^+)_{12}(U^{5+})_2(S^{2-})_{13}(S^{1-})_2$. Each could lead to p-type metallic behavior due to the delocalization of S^{1-} holes in the valence band. Because each formalism has a different number of unpaired electrons on the U ions, the magnitude of the material's paramagnetic response can be used to elucidate the correct oxidation state formalism. (Being delocalized, the S^{1-} states would be magnetically silent.)

Magnetic susceptibility studies: The temperature-dependent magnetic susceptibility of $K_6Cu_{12}U_2S_{15}$, taken at 5000 G over the range 5–300 K, is shown in Figure 6. The data were

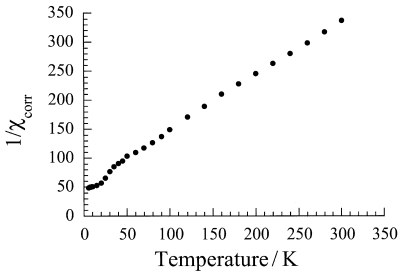

Figure 6. Inverse molar magnetic susceptibility plotted against temperature for $K_6Cu_{12}U_2S_{15}$ at 5000 G. The data have been corrected for Pauli paramagnetism ($\chi_M^{corr} = \chi_M - \chi_{TIP}$).

corrected for Pauli paramagnetism by applying a χ_{TIP} value of 0.0008 emu mol^{-1}. Curie–Weiss behavior is evident between 300–100 K with local antiferromagnetic ordering indicated. Below 100 K, there is a slight negative deviation from the straight line extrapolated from higher temperatures. This phenomenon can be attributed to crystal-field splitting common to U cations,[21] although since the deviation is modest, only a weak crystal-field effect can be inferred. At $\sim$30 K, a small but noticeable ferromagnetic "dip" is also observed, but its unclear whether or not this represents an actual transition, since the data level off again at 20 K.

A linear curve fit to the data above 100 K gives a μ_{eff} of 2.96(2) μ_B per formula and a Weiss constant, θ, of $-69(4)$ K. Dividing the μ_{eff} by $\sqrt{2}$ (since μ_{eff} varies as the square root of χ_m) yields 2.09(2) μ_B for each U in the formula. This value is lower than both the theoretical calculations for a $5f^2$ U^{4+} ion (3.58 μ_B)[22] and experimentally observed μ_{eff} values for several solid-state transition metal/U^{4+}/chalcogenides (3.0–3.6 μ_B).[23] It is closer to the expected value for a U^{5+} system.[24] This suggests that an unequivocal assignment of the oxidation state of U based on the magnetic data would be challenging.

In order to get an indication of probable oxidation states, we have used two different computer programs, namely EUTAX and VALENCE,[25] to perform bond valence sums, (the only difference between these two methods is that they adopt different R_o values in the calculation). The results from both programs suggest U^{5+} as the likely oxidation state. The results from EUTAX give valence sums at U(1) = 5.182, Cu(1) = 1.084, S(1) = −1.92, S(2) = −1.73. Those from VALENCE give valence sums at U(1) = 5.046, Cu(1) = 1.088, S(1) = −1.682, S(2) = −2.00. Interestingly, the bond valence sum calculations favor the presence of U^{5+} in the structure. It is also interesting that the average bond valence of the sulfur atoms is slightly less than −2; this implies some electron deficiency on these sites.

Any formalism, regardless of U^{4+} or U^{5+} preference, requires that S^{1-} states (holes) are delocalized over all sulfur atoms. The next logical question is whether such delocalized S^{1-} states give rise to metallic behavior, or some mechanism is retarding carrier mobility (see section on charge transport below).

Charge-transport measurements: Although $K_6Cu_{12}U_2S_{15}$ single crystals of sufficient size for diffraction studies were obtained, growing specimens large enough to easily attach contacts for charge-transport measurements has remained elusive. As such, these experiments were performed on polycrystalline pellets compacted at 270 °C.

Figure 7a shows representative electrical conductivity data for a polycrystalline pellet as a function of temperature. The conductivity decreases with increasing temperature, a behavior characteristic of a metal. That this is observed in polycrystalline pellets despite the inherent high degree of grain boundaries, which would impede carrier mobility, is testament to the strongly conducting nature of the sample. For the sample compacted at room temperature, the average conductivity of 300 K is $\sim$50 S cm^{-1}. Hot pressing the pellets reduces the resistance due to grain boundaries and results in a thirty-fold increase in the conductivity at 300 K to give values in excess of 1500 S cm^{-1}. At 6 K, the conductivity reaches a value of 7500 S cm^{-1}. In general, polycrystalline pellets are 10–1000 times less conductive than single crystals, and so the actual conductivity of $K_6Cu_{12}U_2S_{15}$ may be still higher.

Thermopower measurements are an excellent complement to conductivity data because the experiments provide additional information on a material's charge-transport behavior, while being independent of grain boundary effects. Figure 7b

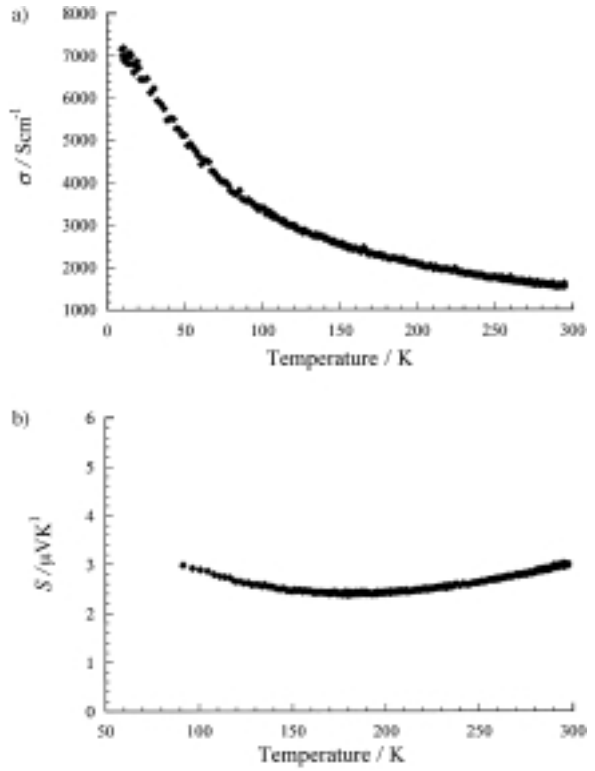

Figure 7. a) The electrical conductivity [$S\,cm^{-1}$] as a function of temperature [K] of polycrystalline pellets of $K_6Cu_{12}U_2S_{15}$ compacted at 270 °C. b) Thermopower [$\mu V\,K^{-1}$] as a function of temperature [K] of polycrystalline pellet of $K_6Cu_{12}U_2S_{15}$ compacted at 270 °C.

shows the Seebeck coefficient (S) as a function of temperature for a hot-pressed polycrystalline pellet of $K_6Cu_{12}U_2S_{15}$. The magnitude of the data is small for both samples ($< 5\ \mu V\,K^{-1}$); this is characteristic of a good metal, and the positive values indicate holes at the charge carriers. The positive slopes above 200 K are also typical of metallic behavior, although the gradual change to a negative slope below 200 K may indicate phonon-drag, as it is typically observed in many metallic systems.[26] The presence of phonon-drag is consistent with the fact that no change in the conductivity data was observed over the same temperature region.

The charge-transport behavior contrasts with the poor conductivity and a non-metallic thermopower of $K_2Cu_2CeS_4$ and $CsCuCeS_3$ mentioned in the introduction. Recall that those phases feature anionic layers that rely on the poorly interacting 4f orbitals of Ce for their extended bonding. In $K_6Cu_{12}U_2S_{15}$, however, the S(2) atoms link [CuS_3] trigonal planes into a three-dimensional network independent of the U atoms. Not only are three-dimensional structures in general less prone to defects, which would disrupt conduction pathways, but the network does not rely on poorly contributing orbitals for its extended band structure. Although not needed to achieve a three-dimensional network, the more covalent U 5f orbitals can only serve to enhance the overall overlap rather than limit conduction pathways, as would the more contracted 4f orbitals of Ce.

One might argue that $K_6Cu_{12}U_2S_{15}$ would tend to greater conductivity because it contains more than one S^{1-} per formula in contrast to the one S^{1-} per formula found for Ce-containing quaternaries. The number of holes per formula, however, is not as germane as their density within the valence band, approximated by the number of holes per sulfur atom (holes/S). If all U^{4+} are used in the oxidation state formalism then $K_6Cu_{12}U_2S_{15}$ has 0.27 holes/S, slightly more than $K_2Cu_2CeS_4$ (0.25 holes/S) but less than $CsCuCeS_3$ (0.33 holes/S). Using all U^{5+} in the formalism leads to an even lower population of holes in the valence band (0.13 hole/S). This emphasizes how the band structure of $K_6Cu_{12}U_2S_{15}$, which arises from the three-dimensional atomic structure, plays a greater role in promoting greater delocalization (i.e., higher mobilities) and higher conductivity.

Conclusion

$K_6Cu_{12}U_2S_{15}$ represents a novel example of an f-element compound with metallic conduction through $S^{2-}/^{1-}$ oxidation states delocalized through the valence band. This is in contrast to the hopping conduction observed earlier in $K_2Cu_2CeS_4$ and $CsCuCeS_3$ and can be largely attributed to the three-dimensional, highly covalent anionic network of $K_6Cu_{12}U_2S_{15}$. To date, this compound with its unusual cubic structure remains unique as the formation of isostructural phases with like-charged metals substituting the Cu or f-block element has not been achieved for any of these quaternary mixed S^{2-}/S^{1-} phases. It would be interesting to attempt to control the electronic properties of this material through hole-annihilation experiments by using methods applied earlier to KCu_4S_3.[27]

Acknowledgement

The authors wish to gratefully acknowledge the National Science Foundation (DMR-9817287 MGK) and (DMR-9622025 CRK) for financial support. This work made use of the SEM facilities of the Center for Electron Optics at Michigan State University.

[1] a) J. C. W. Folmer, F. Jellinek, *J. Less Common Met.* **1980**, *76*, 153 – 159; b) R. V. Baranova, Z. G. Pinsker, *Zh. Strukt. Khim.* **1970**, *11*, 690 – 694; c) R. V. Baranova, Z. G. Pinsker, *Kristallografiya* **1973**, *18*, 1169 – 1173.

[2] D. B. Brown, J. A. Zubieta, P. A. Vella, J. T. Wrobleski, T. Watt, W. E. Hatfield, P. Day, *Inorg. Chem.* **1980**, *19*, 1945 – 1950.

[3] X. Zhang, T. Hogan, C. R. Kannewurf, M. G. Kanatzidis, *J. Am. Chem. Soc.* **1996**, *118*, 693 – 694.

[4] a) Z. Peplinski, D. B. Brown, T. Watt, W. E. Hatfield, P. Day, *Inorg. Chem.* **1982**, *21*, 1752 – 1755; b) C. Burschka, *Z. Naturforsch. B* **1979**, *34*, 396 – 397.

[5] Other examples of ternary Q^{2-}/Q^{1-} compounds include $A_3Cu_8S_6$ (A = K, Rb): a) see ref. [4b]; b) L. W. terHaar, F. J. DiSalvo, H. E. Bair, R. M. Fleming, J. V. Waszczak, W. E. Hatfield, *Phys. Rev. B* **1987** *35*, 1932 – 1938; c) R. M. Fleming, L. W. terHaar, F. J. DiSalvo, *Phys. Rev. B* **1987** *35*, 5388 – 5391; $A_3Cu_8Se_6$, (A = Rb,Cs): d) H. Schils, W. Bronger, *Z. Anorg. Allg. Chem.* **1979** *456*, 187 – 193; $Cs_2Cu_5Se_4$: e) W. Bronger, H. Schils, *J. Less Common Met.* **1982** *83*, 279 – 285; $TlCu_2Q_2$, (Q = S, Se): f) R. Berger, C. F. Van Bruggen, *J. Less Common Met.* **1984**, *99*, 113 – 123; g) R. Berger, *J. Less Common Met.* **1989**, *147*, 141 – 148; $TlCu_6S_4$: h) R. Berger, L. Eriksson, *J. Less Common Met.* **1990**, *161*, 165 – 173; $Tl_5Cu_{14}Se_{10}$: i) R. Berger, A. Meerschaut *Eur. J. Solid State Inorg. Chem.* **1988**, *25*, 279 – 288.

  0947-6539/00/0609-1606 $ 17.50+.50/0

[6] W. Rüdorff, H. G. Schwarz, M. Walter, *Z. Anorg. Allg. Chem.* **1952**, *269*, 141–149.
[7] A. C. Sutorik, J. Albritton-Thomas, C. R. Kannewurf, M. G. Kanatzidis, *J. Am. Chem. Soc.* **1994**, *116*, 7706–7713.
[8] A. C. Sutorik, J. Albritton-Thomas, T. Hogan, C. R. Kannewurf, M. G. Kanatzidis, *Chem. Mater.* **1996**, *8*, 751–761.
[9] A polaron is simply a charge carrier, be it electron or hole, which is trapped in the potential that it induces in the field around it. The mobility of the carrier is then limited by having to overcome the induced field around it; this leads to a hopping conduction mechanism: P. Dougier, J. C. C. Fan, J. B. Goodenough, *J. Solid State Chem.* **1975**, *14*, 247–259.
[10] F. Feher, *Handbuch der Präparativen Anorganischen Chemie* (Ed.: G. Brauer), Fedinand Enke, Stuttgart (Germany), **1954**, pp. 280–281.
[11] A. C. Sutorik, M. G. Kanatzidis, *J. Am. Chem. Soc.* **1997**, *119*, 7901–7902.
[12] J. W. Lyding, H. O. Marcy, T. J. Marks, C. R. Kannewurf, *IEEE Trans. Instrum. Meas.* **1988**, *37*, 76–80.
[13] H. O. Marcy, T. J. Marks, C. R. Kannewurf, *IEEE Trans. Instrum. Meas.* **1990**, *39*, 756–760.
[14] G. M. Sheldrick, *SHELXTL: Version 5.0*, Siemens Analytical X-ray Systems, Madison, WI 53719 (USA), **1994**.
[15] R. Lelieveld, D. J. W. Ijdo, *Acta Crystallogr. Sect. B* **1980**, *36*, 2223–2226.
[16] a) K. Takeuchi, Y. Kodoh, G. Sato, *Z. Kristallogr.* **1985**, *173*, 119–128; b) H. Fjellvag, F. Gronvold, S. Stolen, A. F. Andresen, R. Mullerkafer, A.Simon, *Z. Kristallogr.* **1988**, *184*, 111–121.
[17] X. Zhang, M. G. Kanatzidis, *J. Am. Chem. Soc.* **1994**, *116*, 1890.
[18] a) H. Noel, M. Potel, *J. Less Common Met.* **1985**, *113*, 11–15; b) N. C. Baenziger, R. E. Rundle, A. I. Snow, A. S. Wilson, *Acta Crystallogr.* **1950**, *3*, 34–40.
[19] a) K. Chondroudis, M. G. Kanatzidis, *J. Am. Chem. Soc.* **1997**, *119*, 2574–2575; b) A. C. Sutorik, M. G. Kanatzidis, *J. Am. Chem. Soc.* **1997**, *119*, 7901–7902.
[20] a) A. C. Sutorik, M. G. Kanatzidis, *Polyhedron* **1997**, *16*, 3921–3927; b) A. C. Sutorik, M. G. Kanatzidis, *J. Am. Chem. Soc.* **1997**, *119*, 7901–7902.
[21] T. H. Siddall III in, *Theory and Applications of Molecular Paramagnetism* (Eds.: E. A. Boudreaux, L. M. Mulay), Wiley, New York, **1976**, p. 306.
[22] N. N. Greenwood, A. Earnshaw, *Chemistry of the Elements*, Pergamon, New York, **1984**, p. 1443.
[23] H. Noel, R. Troc, *J. Solid State Chem.* **1979**, *27*, 123.
[24] A. J. Freeman, C. Keller, *Handbook on the Physics and Chemistry of the Actinides*, *Vol. 6*, New York, **1991**, pp. 337–366.
[25] a) The valence sum rule derives from Pauling's second rule, which has been used by mineralogists as a test for the correctness of a structure. L. Pauling, *J. Am. Chem. Soc.* **1929**, 51, 1010–1026; b) I. D. Brown, *J. Appl. Crystallogr.* **1996**, *29*, 479–480.
[26] F. J. Blatt, *Thermoelectric Power of Metals*; Plenum, New York, **1976**.
[27] F. Viola, R. Schollhorn, *J. Chem. Soc. Chem. Commun* **1992**, *12*, 907–908.

Received: May 17, 1999
Revised version: November 15, 1999 [F1792]